Topographic controls on gravity currents in porous media

Samuel S. Pegler[1,†], **Herbert E. Huppert**[1,2,3] **and Jerome A. Neufeld**[1,4]

[1]Institute of Theoretical Geophysics, Department of Applied Mathematics and Theoretical Physics, University of Cambridge, Wilberforce Road, Cambridge CB3 0WA, UK

[2]Faculty of Science, University of Bristol, Bristol BS8 1UH, UK

[3]School of Mathematics and Statistics, University of New South Wales, Sydney 2052, Australia

[4]BP Institute and Department of Earth Sciences, University of Cambridge, Madingley Road, Cambridge CB3 0EZ, UK

We present a theoretical and experimental study of the propagation of gravity currents in porous media with variations in the topography over which they flow, motivated in part by the sequestration of carbon dioxide in saline aquifers. We consider cases where the height of the topography slopes upwards in the direction of the flow and is proportional to the nth power of the horizontal distance from a line or point source of a constant volumetric flux. In two-dimensional cases with $n > 1/2$, the current evolves from a self-similar form at early times, when the effects of variations in topography are negligible, towards a late-time regime that has an approximately horizontal upper surface and whose evolution is dictated entirely by the geometry of the topography. For $n < 1/2$, the transition between these flow regimes is reversed. We compare our theoretical results in the case $n = 1$ with data from a series of laboratory experiments in which viscous glycerine is injected into an inclined Hele-Shaw cell, obtaining good agreement between the theoretical results and the experimental data. In the case of axisymmetric topography, all topographic exponents $n > 0$ result in a transition from an early-time similarity solution towards a topographically controlled regime that has an approximately horizontal free surface. We also analyse the evolution over topography that can vary with different curvatures and topographic exponents between the two horizontal dimensions, finding that the flow transitions towards a horizontally topped regime at a rate which depends strongly on the ratio of the curvatures along the principle axes. Finally, we apply our mathematical solutions to the geophysical setting at the Sleipner field, concluding that topographic influence is unlikely to explain the observed non-axisymmetric flow.

Key words: gravity currents, porous media, topographic effects

1. Introduction

Gravity-driven flows in porous media have an extensive range of applications in the Earth sciences and in industry. These include the flow of groundwater, oil and gas through porous geological formations. Our interest here stems principally from the

† Email address for correspondence: ssp23@cam.ac.uk

developing technology of carbon-dioxide (CO_2) sequestration, whereby carbon dioxide is injected at high pressure into a porous aquifer deep underground (Orr 2009). In such environments, the CO_2 is of lower density than the ambient brine, causing it to rise under the influence of buoyancy and eventually spread below an impermeable caprock. The feasibility of this technology depends on the containment of CO_2 within the aquifer. In this article, we explore the fluid mechanics that governs the spread of CO_2, focusing on understanding the influence of variations in the height of the overlying caprock on the dynamics of the flow.

At the Sleipner field, where this technology is currently in operation, the vertical position of the caprock varies gradually by a few metres over horizontal scales of hundreds of metres, forming a dome-shape structure centred on the point of injection. Above the point of injection, where the topography of the caprock is effectively horizontal, the leading-order propagation of the current can be described by an axisymmetric similarity solution (Lyle *et al.* 2005; Bickle *et al.* 2007). Vella & Huppert (2006) showed that this similarity solution applies at early times even if the topography is sloped to any angle of inclination. At later times, the influence of variations in the topography cause the current to depart from axisymmetric flow. At Sleipner, the currents of CO_2 have been observed to deviate significantly from axisymmetric flow and it has been proposed that these deviations are caused by the variations in the topography (Arts *et al.* 2008; Boait *et al.* 2012). Boait *et al.* (2012) also suggested that the topography may cause the flow to transition towards a regime in which the surface of the current is close to horizontal. Our focus in this paper is to address the evolution towards such a regime, in which the extent of the current ultimately becomes controlled only by geometry and the total volume of fluid injected.

To date, theoretical studies of gravity currents in porous media have typically focused on cases where the topography is horizontal (Huppert 1986; Bear 1988; Barenblatt 1996; Lyle *et al.* 2005; Mitchell & Woods 2006; Nordbotten & Celia 2006; Hesse *et al.* 2007) or of constant slope (Huppert & Woods 1995; Vella & Huppert 2006; Gunn & Woods 2011; de Loubens & Ramakrishnan 2011). By applying thin-film approximations, these authors show how the predominantly parallel flow can become driven either by gradients in hydrostatic pressure or by the component of gravity parallel to the slope. The influence of three-dimensional topographic variations has been considered by Golding & Huppert (2010), who analysed the flow in a channel of uniform cross-section. These authors calculated similarity solutions to their model equations, which are derived under the presupposition that the flow is unidirectional and that the vertical position of the interface does not vary across the width of the channel.

Here, we extend these earlier studies by considering the case of topography that confines the flow and by allowing for three-dimensional topography that varies in the horizontal dimensions, forming a basin. In such configurations, a new feature of convergence towards states controlled by the variations in the topography can occur, and we investigate this in the context of the two- and three-dimensional flows produced at a constant rate by a line or point source, respectively. A focus of our analysis is to determine the time scales associated with the transitions towards such topographically controlled states. We compare our theoretical predictions with data from a series of laboratory experiments, extending previous experimental studies (Huppert & Woods 1995; Vella & Huppert 2006; Golding & Huppert 2010) by addressing the case of topography that slopes upwards in the direction of the flow.

We begin in §2 by reviewing our model of a thin gravity current in a porous medium with variations in the topography along which it flows. We proceed in
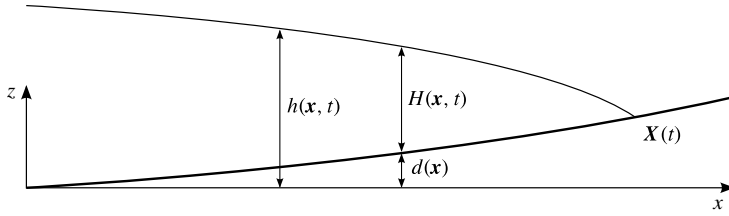
FIGURE 1. Schematic of a gravity current of height $h(x, t)$ and thickness $H(x, t)$ in an infinitely deep porous medium over variable topography described by $d(x)$.

§3 to calculate solutions to the model equations in the case of a two-dimensional current produced by a line source. The theoretical predictions are then compared with the results of a series of laboratory experiments. In §4, we consider the three-dimensional flow due to a point source, focusing on cases where the topography is either axisymmetric or paraboloidal. Finally, in §5 we apply our mathematical solutions to the geophysical setting of the Sleipner field, with the aim of assessing the importance of topographic variations on the propagation of the CO_2.

2. Theoretical model

Consider the gravity-driven propagation of an incompressible viscous fluid of density ρ and dynamic viscosity μ in a porous medium of homogeneous porosity ϕ and permeability k, which flows in the effectively infinite region above a rigid, impermeable boundary given by $z = d(x)$, where $x \equiv (x, y)$ (see figure 1). Let $z = h(x, t)$ and $H(x, t) \equiv h - d$ denote the height of the interface of the current (assumed sharp) and the thickness of the current, respectively. We assume that both the gradient of the lower boundary and that of the interface of the current remain small at all times, so ∇h and $\nabla d \ll 1$, where we use ∇ to denote the horizontal gradient operator. Under these assumptions, the flow is predominantly horizontal and, by integration of the vertical Darcy equation, the pressure can be approximated as hydrostatic to leading order (Huppert 1986; Bear 1988; Huppert & Woods 1995; Lyle *et al.* 2005; Vella & Huppert 2006; Neufeld, Vella & Huppert 2009; Golding & Huppert 2010), so

$$p \sim p_0(x, t) - \rho g(z - h) \quad (\nabla d, \nabla h \ll 1), \tag{2.1}$$

where $p_0(x, t)$ is a constant of integration representing the pressure along the interface and g is the acceleration due to gravity. The assumption of hydrostatic pressure (2.1) can be expected to hold uniformly throughout the currents described here, save in a narrow region around the point of injection (Lyle *et al.* 2005; Pegler *et al.* 2013).

In the limit where the depth of the current is much less than the depth of the aquifer (e.g. Bear 1988; Huppert & Woods 1995; Barenblatt 1996; Lyle *et al.* 2005; Vella & Huppert 2006; Golding & Huppert 2010), the pressure in the ambient fluid can be approximated as a constant p_0 to leading order, in which case (2.1) simplifies to

$$p = p_0 - \rho g(z - h). \tag{2.2}$$

We also focus on this case, which can be expected to provide a good approximation to many geophysical settings (Sleipner being one proposed example; Bickle *et al.* 2007), and as an instructive example on which to begin fluid mechanical analysis of non-trivial topography.

By substituting (2.2) into the horizontal component of the Darcy equation, we find that the horizontal velocity is independent of z and given by

$$\boldsymbol{u} = -U\nabla h, \tag{2.3}$$

where $U \equiv \rho g k/\mu$ is the natural buoyancy velocity of the fluid. Substituting (2.3) into the depth-integrated form of the continuity equation, we obtain the governing nonlinear diffusion equation

$$\phi\frac{\partial h}{\partial t} = U\nabla \cdot (H\nabla h). \tag{2.4}$$

In the case of a broad, linear slope ($d = ax$), Vella & Huppert (2006) showed how the contribution to the divergence of flux in (2.4) due to the along-slope component of gravity, $U\nabla H \cdot \nabla d$, eventually dominates the dynamics of the current downstream of the source. Unidirectional flows in which this component of gravity is assumed to be dominant from the outset have been considered by Huppert & Woods (1995) and Golding & Huppert (2010), where (2.4) reduces to a simple wave equation. In cases where the topography slopes upwards in the direction of the flow, such as those addressed in this paper, the contribution to (2.4) due to the along-slope component of gravity can, by contrast, never become dominant. This reflects the fact that the along-slope component of gravity can only drive the current downhill. In order to flow uphill, the current must instead rely on the development of gradients in hydrostatic pressure, represented by the diffusive contribution $UH\nabla^2 h$ to the right-hand of side of (2.4).

In common with previous models (e.g. Huppert 1986), we assume that the frontal thickness is zero and that its position evolves kinematically according to

$$H = 0, \quad \phi\dot{X} = -U\nabla h \quad (\boldsymbol{x} = \boldsymbol{X}), \tag{2.5a,b}$$

where $X(t)$ denotes a location on the edge of the current and the dot denotes d/dt.

3. Line source

We begin by considering the two-dimensional flow over topography described by a power law $d(x) = ax^n$, where $n \geqslant 0$ is the *topographic exponent* and $a > 0$ is the *topographic scale*. This expression for d describes a class of geometries, allowing for convex surfaces ($n > 1$), linear slopes ($n = 1$) and concave surfaces ($n < 1$). The flow of the current is governed by the two-dimensional form of (2.4), namely,

$$\phi\frac{\partial h}{\partial t} = U\frac{\partial}{\partial x}\left(H\frac{\partial h}{\partial x}\right) \quad \text{where } H \equiv h - ax^n. \tag{3.1}$$

We consider solutions to this equation subject to (2.5a,b) and the source condition

$$-\phi UH\frac{\partial h}{\partial x} = q \quad (x = 0), \tag{3.2}$$

which implies a delivery of fluid at the constant volumetric rate per unit width q, assumed to initiate at $t = 0$.

By considering the scaling $h \sim d = ax^n$ in (3.1) and (3.2), we determine the scales

$$\mathscr{L} \equiv \left(\frac{q}{a^2\phi U}\right)^{1/(2n-1)}, \quad \mathscr{T} \equiv \frac{\phi\mathscr{L}^{2-n}}{aU}, \quad \mathscr{H} \equiv a\mathscr{L}^n, \tag{3.3a,b,c}$$

which characterize the horizontal extent, time and thickness at which the thickness of the current becomes comparable to the change in the height of the topography across its extent. Note that the length scale (3.3a) cannot be formed if $n = 1/2$ or $a = 0$, which reflects the existence of similarity solutions in these cases. For other values of n and a, the flow cannot be described by a single similarity solution that is valid for all time, instead undergoing a transition between certain flow regimes over a length scale characterized by (3.3a), as we shall explore below. The corresponding time scale of this transition (3.3b) is notably independent of the entry flux q in cases where the topography is parabolic ($n = 2$).

We use (3.3a,b,c) to make the system dimensionless according to

$$x \equiv \mathcal{L}\hat{x}, \quad t \equiv \mathcal{T}\hat{t}, \quad (h, H) \equiv \mathcal{H}(\hat{h}, \hat{H}). \tag{3.4}$$

In terms of (3.4), and with hats dropped, (2.5a,b) become

$$\frac{\partial h}{\partial t} = \frac{\partial}{\partial x}\left(H\frac{\partial h}{\partial x}\right) \quad \text{where } H \equiv h - x^n, \tag{3.5a,b}$$

and conditions (3.2) and (2.5a,b) become

$$-H\frac{\partial h}{\partial x} = 1 \qquad (x = 0), \tag{3.6}$$

$$H = 0, \quad \dot{X} = -\frac{\partial h}{\partial x} \quad (x = X), \tag{3.7a,b}$$

respectively. Equations (3.5)–(3.7) are together consistent with the volume constraint

$$\int_0^X H\,dx = t. \tag{3.8}$$

The dimensionless system above depends only on the topographic exponent n.

With horizontal topography ($n = 0$), Huppert (1986) showed that (3.5)–(3.8) support a similarity solution of the form

$$H = t^{1/3}f(x/X), \quad X = \xi_N t^{2/3}, \tag{3.9a,b}$$

where $\xi_N \approx 1.48$ and $f(x/X)$ is a function that can be determined numerically from the solution of an ordinary differential equation. As noted above, however, non-horizontal slopes ($n > 0$) do not generally permit such a similarity solution (with the unique exception of $n = 1/2$, discussed later). For such n, we instead solve the system (3.5)–(3.7) numerically using a partially implicit, finite-difference scheme of second order, in which the coefficient of diffusion in (3.5) is treated explicitly, with variable time steps and initialized using early-time asymptotic solutions obtained below. In our numerical scheme, the time-dependent domain of the current $[0, X(t)]$ is transformed to a steady domain by recasting the system of equations in terms of the scaled coordinate system (ζ, t), where $\zeta \equiv x/X$.

A suite of illustrative numerical solutions obtained in this manner for $n = 1/4, 1/2, 1$ and 2 are shown as thin, solid curves in figures 2(a)–2(d), respectively, and the corresponding evolutions of the frontal positions are shown in the last three of these cases in figure 3. For both $n = 1$ and 2, the flow transitions from the similarity solution (3.9) towards a regime with an approximately horizontal free surface. With $n = 1/4$, the transition between these two flow regimes is reversed; with $n = 1/2$, neither of these regimes applies in any asymptotic limit of time. We proceed to analyse these transitions.
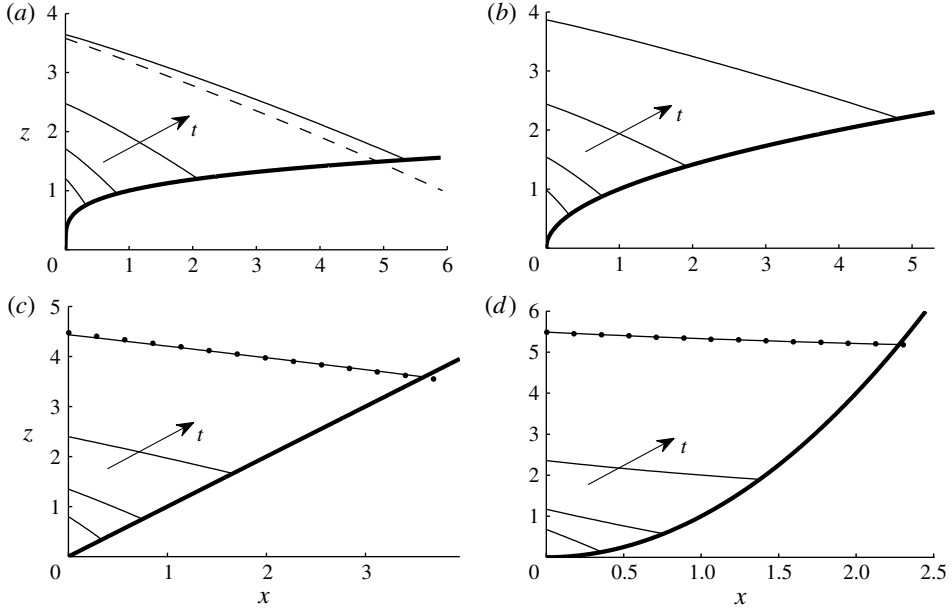
FIGURE 2. The numerically obtained evolution of the height $h(x, t)$ of the two-dimensional current produced by a line source along $x = 0$, shown at dimensionless times $t = 0.125, 0.5, 2$ and 8, for topographic exponents of (*a*) $n = 1/4$, (*b*) $1/2$, (*c*) 1 and (*d*) 2. The similarity solution (3.9), which provides a late-time asymptote in cases with $n < 1/2$, is shown in (*a*) at $t = 8$ (dashed). The asymptote passes through the lower boundary (bold) because its construction does not involve an exact imposition of the condition of vanishing frontal thickness (3.7*a*). The topographically controlled state composed of the leading-order horizontally topped state along with its first-order correction (3.13) is shown in both (*c*) and (*d*) at $t = 8$ (dotted). Again, the asymptote passes through the lower surface because (3.7*a*) is only imposed to first order as part of its construction.

For topographic exponents of $n > 1$, there is a region close to the source ($0 \leqslant x \leqslant X \ll 1$) where the topography can be treated as horizontal at early times ($t \ll 1$). Hence, the similarity solution (3.9) that describes the flow in the case of horizontal topography can be expected to provide an early-time asymptote for the flow if $n > 1$. This is confirmed by the fact that our numerically obtained frontal position $X(t)$ in the case $n = 2$ approaches that of the similarity solution (3.9*b*) in the limit $t \to 0$, illustrated in figure 3. In fact, (3.9) describes the early-time flow more generally for $n > 1/2$, which is perhaps surprising because this range includes some values ($1/2 < n < 1$) for which the topography approaches an infinite slope near the source. For such n, (3.9) provides an early-time asymptote because the thickness of the current H implied by (3.9*a*) still remains asymptotically larger than the total change in the height of the topography experienced by the current, $d(X) - d(0)$. That is,

$$\left[H = t^{1/3} f(x/X) \right] \gg \left[d(X) - d(0) = \xi_N^n t^{2n/3} \right] \quad (t \to 0) \tag{3.10}$$

if and only if $n > 1/2$. Like the case $n = 2$, the approach of the frontal position $X(t)$ towards that implied by the early-time asymptote (3.9*b*) is illustrated by our numerical solution for $n = 1$ in figure 3.

In the critical case $n = 1/2$, both sides of (3.10) are of equal order at all times, so the asymptotic relationship of (3.10) does not apply. The similarity solution (3.9)
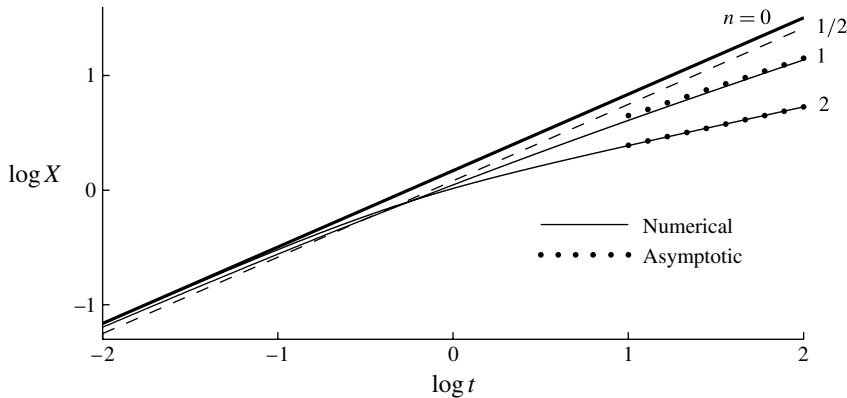
FIGURE 3. The evolution of the frontal position $X(t)$ for $n = 0$ (bold), $n = 1/2$ (dashed) and $n = 1$ and 2 (each thin) as a function of time. The cases $n = 0$ and $n = 1/2$ are each described analytically by a similarity solution of the form (3.9*b*), with different prefactors $\xi_N \approx 1.48$ and 1.21, respectively. The solutions for $n = 1$ and 2, which we have determined numerically, are seen to evolve from the similarity solution (3.9*b*) at early times towards the asymptote (3.11*b*) (dotted) at late times. This illustrates a transition towards a regime in which the top surface of the current has become close to horizontal.

cannot therefore provide an asymptote for the flow in any limit of time. Instead, the non-existence of the length scale (3.3*a*) in this case indicates that the flow can be described exactly by a different similarity solution, of identical form to (3.9), but with a different function f for the thickness distribution and the smaller frontal coordinate $\xi_N \approx 1.21$. For this unique case, shown by our numerical solution in figure 2(*b*), the influence of hydrostatic spreading and topographic variations are comparable at all times.

For yet more concave surfaces ($n < 1/2$), the asymptotic relationship of (3.10) instead holds in the opposite limit of large time ($t \to \infty$), implying that the similarity solution (3.9) provides a late-time asymptote for the flow. The late-time convergence towards (3.9) is illustrated for the case $n = 1/4$ in figure 2(*a*), which shows the approach of our numerical solution (solid curves) towards the similarity solution (3.9) (dashed). Note that the similarity solution passes through the lower surface because it is only a leading-order asymptote and does not satisfy the condition of a vanishing frontal thickness (3.7*b*) exactly.

The two cases $n = 1$ and 2 were seen in figure 2(*c,d*) to converge at late times towards a state with an approximately horizontal upper surface. As this transition occurs, the development of an approximately horizontal top implies that the propagation of the extent of the current eventually becomes determined only by geometry and the total volume of injected fluid (3.8). An explicit consideration of the fluid-mechanical balance between gradients in hydrostatic pressure and viscous stresses underlying the self-similar, early-time flow described by (3.9) are no longer required in order to determine the leading-order frontal position. By setting the height of the current to be purely horizontal, so $h = h_0(t)$, applying the volume constraint (3.8) and using (3.7*a*), we determine the height and extent of the horizontally topped regime as

$$h = h_0(t) \equiv \left[\frac{(n+1)}{n} t \right]^{n/(n+1)}, \quad X = X_0(t) \equiv \left[\frac{(n+1)}{n} t \right]^{1/(n+1)}, \quad (3.11a,b)$$
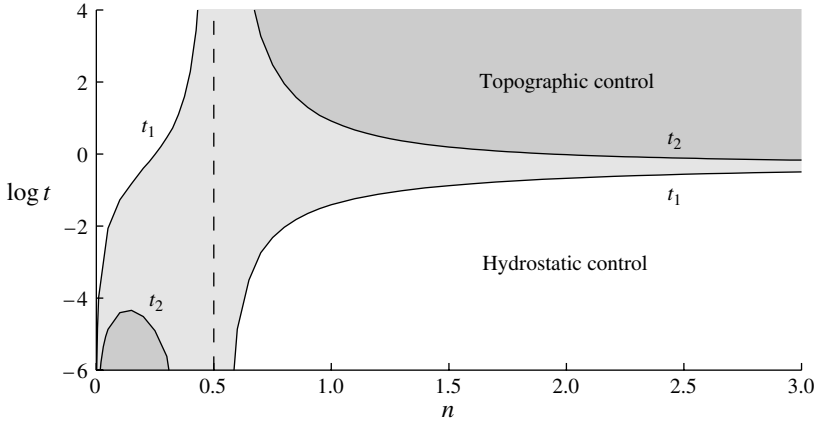
FIGURE 4. Characteristic dimensionless times t_1 and t_2, defined by (3.12*a,b*), at which the flow transitions from the early-time similarity solution (3.9) to the late-time horizontally topped regime (3.11) for $n > 1/2$; the transition is reversed for $n < 1/2$. Times at which the flow is controlled by hydrostatic spreading (white) and topography (heavily shaded) are separated by an intermediate region (lightly shaded) in which both hydrostatic and topographic controls are comparable.

respectively. The late-time convergence of our numerical solutions towards the spreading rate implied by (3.11*b*) is illustrated for the two cases of $n = 1$ and 2 (both of which satisfy $n > 1/2$) in figure 3, where the relationship (3.11*b*) is shown as a dotted line.

   The characteristic dimensionless times at which the frontal position departs from (3.9*b*) and converges towards (3.11*b*) can be seen to vary significantly between the two cases of $n = 1$ and 2. To illustrate this variation across n in more detail, we consider the times t_1 and t_2 that satisfy

$$X(t_1) = 0.9\,\xi_N t_1^{2/3}, \quad X(t_2) = 0.9\,X_0(t_2), \qquad (3.12a,b)$$

which define the times at which the frontal extent is equal to 90% of that implied by the similarity solution (3.9) and by the horizontally topped regime (3.11), respectively. As shown by the solid curves in figure 4, these characteristic transition times are both order unity for $n \gtrsim 2$. However, t_1 decreases by an order of magnitude to the much smaller value $t_1 \approx 4 \times 10^{-2}$ in the case $n = 1$, indicating that the slope of the topography has essentially immediate significance at such n. Meanwhile, the characteristic time of convergence towards the horizontally topped state t_2 increases by an order of magnitude to about $t_2 \approx 10$ in the case $n = 1$, implying a much larger intermediate interval $(t_2 < t < t_1)$ in which the influence of topographic variations is significant but not dominant. The duration of this intermediate interval continues to expand as n is decreased, eventually tending to infinity in the case $n = 1/2$, as neither (3.9) nor (3.11) apply at any stage of the evolution at that value. For $n < 1/2$, $t_2 < t_1$, reflecting the reversal in the order in which the flow transitions between the hydrostatically and topographically controlled regimes. The time to transition away from the horizontally topped regime is very short for all $n < 1/2$, with a maximum value of $t_2 \approx 4 \times 10^{-5}$ occurring at $n \approx 0.1$. In contrast, the characteristic time t_1 of transition towards the similarity solution (3.9*a,b*) varies significantly between different

values of n, with a very slow transition ($t_1 \to \infty$) in the limit $n \to (1/2)^-$, but a rapid transition ($t_1 \to 0$) in the limit of near-horizontal topography, $n \to 0$.

3.1. *Convergence towards or departure from topographic control*

To explore the evolution of the system towards topographic control (3.11) in more detail, we consider the evolution of a small perturbation to it. Specifically, we set

$$h \sim h_0(t)[1 + t^{-\alpha}F(\eta)], \quad X \sim X_0(t)[1 + Kt^{-\beta}], \qquad (3.13a,b)$$

where α and β are exponents of relative decay (to be determined as functions of n), K is a constant, $\eta \equiv x/X_0(t)$ and the asymptotic limit is that of $t^{-\alpha} \to 0$ or, equivalently, $t \to \infty$ if $\alpha > 0$ and $t \to 0$ if $\alpha < 0$. The function $F(\eta)$ in (3.13a) represents the leading-order shape of the current, as a perturbation from the horizontally topped state (3.11a). By substituting (3.13a,b) into (3.5) and (3.8), and neglecting higher-order terms in $t^{-\alpha}$, we determine that

$$\alpha = \frac{2n-1}{n+1}, \quad N = \frac{\mathrm{d}}{\mathrm{d}\eta}\left[(1-\eta^n)\frac{\mathrm{d}F}{\mathrm{d}\eta}\right], \quad \int_0^1 F \, \mathrm{d}\eta = 0, \qquad (3.14a,b,c)$$

where $N \equiv [n/(n+1)]^{\alpha}$ is a constant. The sign of the exponent of relative decay (3.14a) is positive if $n > 1/2$ and negative if $n < 1/2$, which is consistent with the respective decay towards or departure from the horizontally topped state (3.11) in these cases.

The simplified governing equation (3.14b) represents a balance between the large-scale, uniformly increasing height of the current implied by (3.11a) on its left-hand side and the small-scale diffusion of the current that supports this increase on its right-hand side. Integration of (3.14b) subject to a regularity condition on F at $\eta = 1$ yields

$$\frac{\mathrm{d}F}{\mathrm{d}\eta} = -N\frac{1-\eta}{1-\eta^n} \quad \text{and hence } F(\eta) = F_0 + N\int_\eta^1 \frac{1-\eta}{1-\eta^n} \, \mathrm{d}\eta, \qquad (3.15a,b)$$

where F_0 is a constant of integration that can be determined up to quadrature by applying (3.14c). A particular feature of these solutions, implied directly by (3.15a), is that the slope of the current increases by a factor of n between the source and the front of the current, so $F'(0) = nF'(1)$, where we have used a prime here to denote $\mathrm{d}/\mathrm{d}\eta$. In particular, the slope of the current increases or decreases with η, depending on whether n is larger than or less than unity, respectively. With a linear slope ($n = 1$), the integrals in (3.14c) and (3.15b) can be evaluated analytically to obtain the closed-form linear solution $F = (1/2 - \eta)/\sqrt{2}$. Likewise, the solution in the case of parabolic topography ($n = 2$) can be obtained as $F = -(2/3)\{1 + \ln[(1+\eta)/4]\}$.

Notably, it has been possible to determine the first-order perturbation to the thickness given by (3.15b) without any reference to the perturbation to the frontal position in (3.13b), with K and β still to be determined. By substituting (3.13a,b) into the condition of vanishing thickness (3.7a), conducting a Taylor expansion in $t^{-\beta}$ and balancing the first-order terms, we determine that $\beta = \alpha$ and

$$X \sim X_0(t)\left(1 + \frac{F(1)}{n}t^{-\alpha}\right). \qquad (3.16)$$

As $n \to 0$, the prefactor to the first-order correction in (3.16) diverges, which is consistent with the fact that the horizontally topped state (3.13) never emerges if the topography is horizontal ($n = 0$).
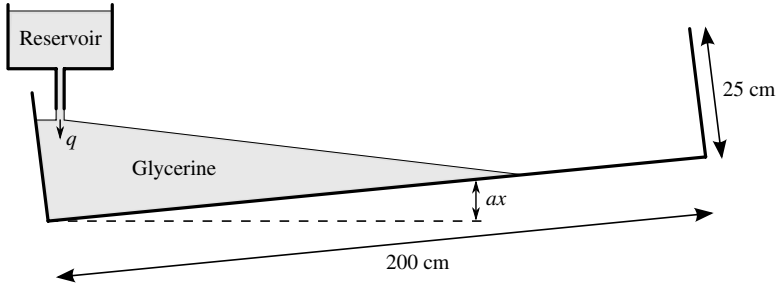
FIGURE 5. Schematic of the experimental Hele-Shaw cell.

As shown by the dotted curves in figure 2(*c,d*), these first-order corrections provide good descriptions of the late-time shape of the current, with a faster rate of converge towards it in the case $n = 2$ compared to the case $n = 1$. Note that the asymptotes slightly overlap the lower boundary because the condition of vanishing frontal thickness (3.7*b*) is imposed only to first-order as part of their construction. The differences in times of transition are consistent with the fact that the rate of convergence is controlled by the exponent of decay (3.14*a*), and this increases with n for $n > 1/2$. Furthermore, the vanishing of α as $n \to 1/2$ is consistent with the fact that the horizontally topped state never emerges in the case $n = 1/2$.

3.2. *Experimental comparison*

We have conducted a series of laboratory experiments with which to compare our theoretical predictions in the case of a linear slope $n = 1$. In common with previous experimental studies (e.g. Huppert & Woods 1995; Neufeld *et al.* 2009), we used a vertical Hele-Shaw cell to model the two-dimensional evolution of a gravity current in a porous medium. With w representing the width of the cell, the equivalence between these flows is given by setting the permeability and porosity equal to $k = w^2/12$ and $\phi = 1$, respectively.

Our experiments were conducted in two different cells formed of two Perspex sheets, each 200 cm long and 25 cm high, but with different mean spacings of $w \approx 1.27 \pm 0.05$ cm and 0.60 ± 0.01 cm. As shown schematically in figure 5, the cell was oriented to a slope a from the horizontal. We used glycerine of density $\rho \approx 1.258 \pm 0.002$ g cm^{-3} and viscosity $\mu \approx 5.0$ to 11.6 g cm^{-1} s^{-1} as the working fluid, which we injected at a constant rate at the lower edge of the cell through a steel pipe connected to a raised reservoir. The constancy of the rate of injection was maintained by keeping the head in the reservoir at a constant level. The density of the glycerine was measured before each experiment using a hydrometer to within an accuracy of ± 0.002 g cm^{-3} and the viscosity of the glycerine was measured using a glass U-tube viscometer to an approximate accuracy of ± 0.1 g cm^{-1} s^{-1}, varying slightly between our experiments owing to differences in water content and temperature. We recorded the experiment using a camera directed towards the front of the Hele-Shaw cell, the results of which were analysed afterwards to determine the evolution of the frontal position $X(t)$ and the entry flux per unit width q by digitally measuring the length and area of the currents in the photographs, respectively. Taking into consideration the resolution of our recorded images, the maximum errors in the digital analysis of the frontal positions were expected to be of the order of 2 cm.
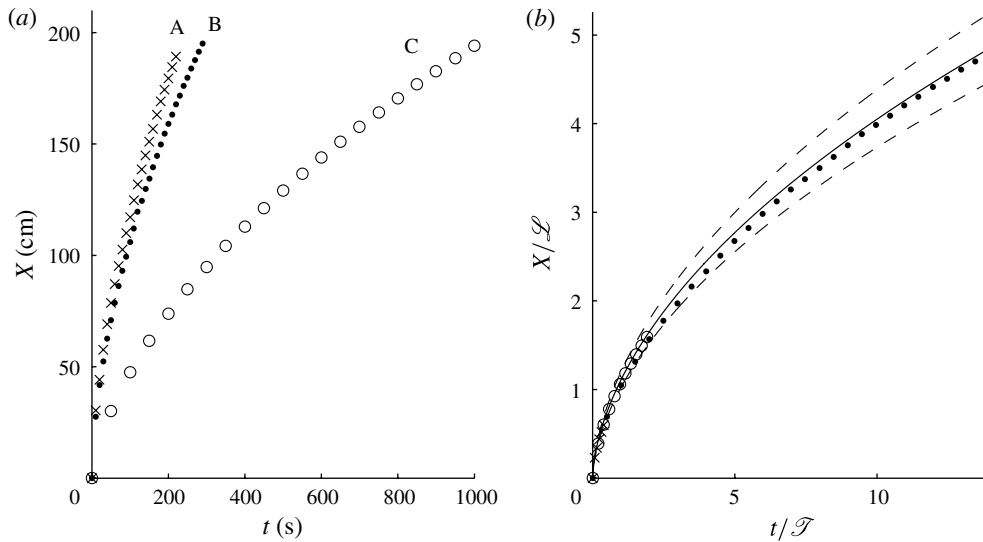
FIGURE 6. (*a*) The raw experimental data for the frontal position $X(t)$ recorded in each of our experiments as a function of time, and (*b*) the same data scaled by the intrinsic length and time scales (3.3*a*,*b*). The errors in measurement of the frontal position were estimated to be smaller than the symbols used in (*a*). In (*b*), the theoretical prediction is shown as a solid curve. The two dashed curves indicate the maximum and minimum theoretical predictions given the tolerances to which we have measured the intrinsic scales $\mathscr{L}$ and $\mathscr{T}$.

Experiment	a	μ (P)	w (cm)	q (cm^2 s^{-1})	Symbol
A	0.040	11.6	1.27	7.2	×
B	0.074	6.2	1.27	5.9	●
C	0.074	11.9	0.60	2.1	○

TABLE 1. Parameter values used in our experiments.

Our experimental parameters spanned slopes of $a = 0.040$ to 0.074, viscosities of $\mu = 6.2$ to 11.9 P, widths of $w = 0.60$ to 1.27 cm and input fluxes per unit width of $q = 2.1$ to 7.2 cm^2 s^{-1} (see table 1). The evolution of the front of each of our experimental currents is plotted in figure 6(*a*) and a time-lapse sequence of images of experiment B is shown in figure 7. On collapsing the data for the evolution of the frontal position in terms of our dimensionless variables (3.4) in figure 6(*b*), we find excellent agreement with the theoretical prediction (solid). Comparison between the position of the experimental interface in figure 7 also shows good agreement with the theoretical prediction (dashed). This provides confirmation that the model gives an accurate description of the dynamics for topography that slopes upwards in the direction of the flow.
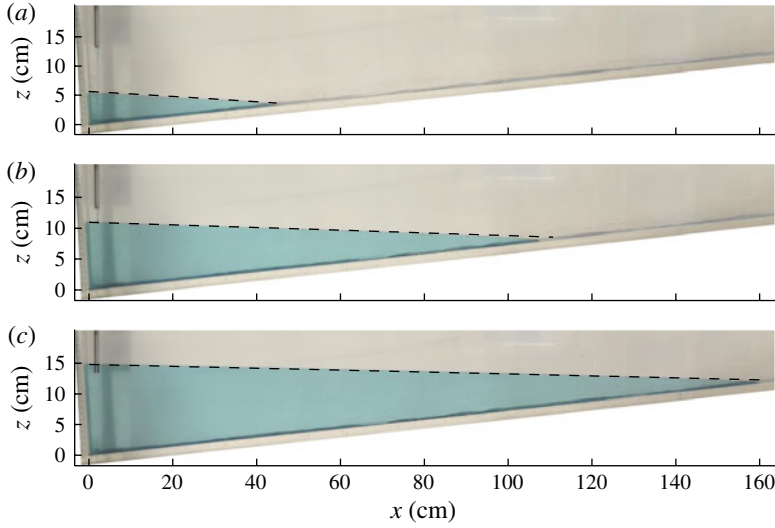
FIGURE 7. (Colour online) Sequence of photographs showing the progression of experiment B at dimensional times (*a*) $t = 20$ s, (*b*) 100 s and (*c*) 200 s. The theoretical prediction for the position of the interface of the current is shown as a dashed curve in each photograph.

4. Point source

We explore the influence of three-dimensional topographic variations by considering topography that can vary in both the *x* and *y* directions. Specifically, we consider two different idealized cases,

$$d(r) = br^n \qquad \text{(axisymmetric)}, \qquad (4.1a)$$

$$d(x, y) = a|x|^m + b|y|^n \quad \text{(three-dimensional)}, \qquad (4.1b)$$

where $a, b \geqslant 0$, corresponding to topography that is axisymmetric or varies with different power laws between the two horizontal dimensions, respectively. Note that (4.1*a*) is a non-trivial special case of (4.1*b*) only if $n = 2$ and $a = b$.

At the origin, we impose the condition of constant injection at a point source,

$$\lim_{r \to 0} \left[-(2\pi\phi U)rH\frac{\partial h}{\partial r} \right] = Q, \qquad (4.2)$$

which implies a radial supply of fluid at the constant volumetric rate Q (cf. Lyle *et al.* 2005; Vella & Huppert 2006). By considering the scalings $h \sim ar^n$ or $h \sim by^n$ in (2.4) and (4.2), we determine the scales of horizontal length, time and thickness,

$$\mathcal{L} \equiv \left(\frac{\mathcal{H}}{b} \right)^{1/n}, \quad \mathcal{T} \equiv \frac{\phi\mathcal{H}^{(2-n)/n}}{Ub^{2/n}}, \quad \mathcal{H} \equiv \left(\frac{Q}{2\pi\phi U} \right)^{1/2}, \qquad (4.3a,b,c)$$

respectively. The thickness (4.3*c*) characterizes the internal thickness of an axisymmetric gravity current supplied at constant flux over a horizontal surface in a deep porous medium (Lyle *et al.* 2005; Vella & Huppert 2006). The length scale (4.3*a*) and time scale (4.3*b*) characterize the extent and time beyond which the topographic variations in the *r*- or the *y*-direction, depending on which of the topographic models (4.1*a,b*) is used, have significant influence on the dynamics of the current. In common

with the time scale in the two-dimensional case (3.3*b*), that of (4.3*b*) is independent of the entry flux when the cross-section of the geometry is parabolic ($n = 2$).

We use (4.3*a,b,c*) to make the system dimensionless according to

$$(x, y) \equiv \mathcal{L}(\hat{x}, \hat{y}), \quad t \equiv \mathcal{T}\hat{t}, \quad H \equiv \mathcal{H}\hat{H}. \tag{4.4}$$

With hats dropped, and in terms of polar coordinates (r, θ), (2.4*a,b*) become

$$\frac{\partial h}{\partial t} = \frac{1}{r} \frac{\partial}{\partial r} \left(r H \frac{\partial h}{\partial r} \right) + \frac{1}{r^2} \frac{\partial}{\partial \theta} \left(H \frac{\partial h}{\partial \theta} \right), \tag{4.5}$$

where the thickness and surface height are related in the two cases (4.1*a,b*) by

$$H = h - r^n \qquad \text{(axisymmetric)}, \tag{4.6a}$$
$$H = h - A|x|^m - |y|^n \quad \text{(three-dimensional)}, \tag{4.6b}$$

respectively. Conditions (4.2) and (2.5*a,b*) become

$$\lim_{r \to 0} \left(-r H \frac{\partial h}{\partial r} \right) = 1, \tag{4.7}$$

$$H = 0, \quad \dot{r}_N = -\frac{\partial h}{\partial r} \quad (r = R), \tag{4.8a,b}$$

where $R(\theta, t)$ is the radial coordinate of the frontal position. Equations (4.5)–(4.8) are together consistent with the volume constraint,

$$\int_0^{2\pi} \int_0^R r H \, \mathrm{d}r \, \mathrm{d}\theta = 2\pi t. \tag{4.9}$$

With axisymmetric topography (4.6*a*), the dimensionless model system above depends only on the topographic exponent n. With the three-dimensional topography (4.6*b*), it also depends on the additional dimensionless parameter

$$A \equiv a b^{-m/n} \mathcal{H}^{(m-n)/n}, \tag{4.10}$$

which measures the relative importance of the variations of the topography between the x- and y-directions. For cases with equal topographic exponents ($m = n$), (4.10) is independent of the fluid-mechanical parameter $\mathcal{H}$, and simplifies to the ratio of the curvatures of the topography between the x- and y-directions, $A = a/b$.

4.1. *Axisymmetric topography*

We begin by considering the axisymmetric case (4.6*a*), in which there is no variation in θ and the second term on the right-hand side of (4.5) is identically zero. With horizontal topography ($n = 0$), Lyle *et al.* (2005) showed that the flow can be described at all times by a similarity solution of the form

$$H = f(r/R), \quad R = \xi_N t^{1/2}, \tag{4.11a,b}$$

where $\xi_N \approx 1.83$ and the function f can be determined numerically from the solution of an ordinary differential equation. As detailed below, such a similarity solution cannot be used to describe cases of $n > 0$ for all time because the influence of topographic variations changes the flow dynamics over a length scale characterized by (4.3*b*). For these cases, we instead solve the system numerically using a scheme similar to that described in § 3.
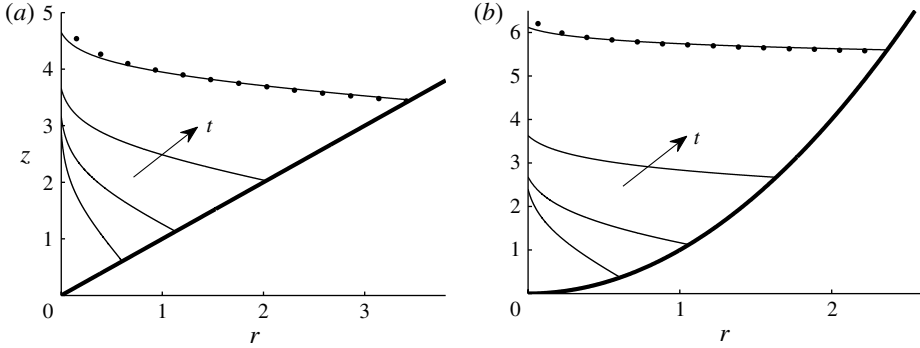
FIGURE 8. The numerically obtained evolution of the height of an axisymmetric current $h(r, t)$ shown at dimensionless times $t = 0.125, 0.5, 2$ and 8 for two topographic exponents, (*a*) $n = 1$ and (*b*) 2. The asymptotic prediction (4.15*b*) is shown at $t = 8$ as a dotted curve in each case. The topography $z = d = r^n$ is shown as a bold curve in each case.

Two illustrative numerical solutions for $n = 1$ and 2 are shown as thin curves in figure 8(*a,b*) and the corresponding evolutions of the frontal positions $X(t)$ are each shown alongside the analytical result (4.11*b*) for $n = 0$ in figure 9. Both the numerical solutions are seen to undergo a similar transition towards a horizontally topped regime as that seen in cases of the two-dimensional problem with $n > 1/2$. Likewise, the similarity solution that applies for horizontal topography (4.11*a,b*) provides a leading-order description of the flow in the limit of small time. Again, we can confirm this mathematically by noting that the thickness of the current H implied by (4.11*a*) is negligible at early times compared to the change in the height of the topography across the extent of the current, $d(R) - d(0)$, implied by (4.11*b*), so

$$[H = f(r/R)] \gg \left[d(R) - d(0) = \xi_N^n t^{n/2} \right] \quad (t \to 0). \quad (4.12)$$

This asymptotic relationship applies for all $n > 0$, confirming that (4.11) describes the early-time flow for all such n. This is different from the two-dimensional case, where the analogue of (3.10) allows for a reversal of the transitions if $0 < n < 1/2$. Again, the form of the horizontally topped state is determined purely from geometry. By setting $h = h_0(t)$ in (4.9) and using the volume constraint (4.8*a*), we determine the height and extent of the late-time horizontally topped regime as

$$h = h_0(t) \equiv \left[\frac{2(n+2)}{n} t \right]^{n/(n+2)}, \quad R = R_0(t) \equiv \left[\frac{2(n+2)}{n} t \right]^{1/(n+2)}, \quad (4.13a,b)$$

respectively. The transition in frontal position from (4.11*b*) towards (4.13*b*) is illustrated by the log–log plot in figure 9.

As in our two-dimensional analysis, we can quantify the variations in the transition times between the asymptotic states of (4.11*b*) and (4.13*b*) by considering the axisymmetric analogues of the transition times (3.12*a,b*), defined by

$$R(t_1) = 0.9 \, \xi_N t^{1/2}, \quad R(t_2) = 0.9 \, R_0(t_2), \quad (4.14a,b)$$

which we plot as functions of n in figure 10. Both t_1 and t_2 are of order unity over a slightly larger range of $n \gtrsim 1$ compared to the two-dimensional case shown in figure 4. In further contrast to the two-dimensional case, the characteristic time of transition away from the similarity solution t_1 attains a minimum of approximately 0.25 at $n \approx 2$.
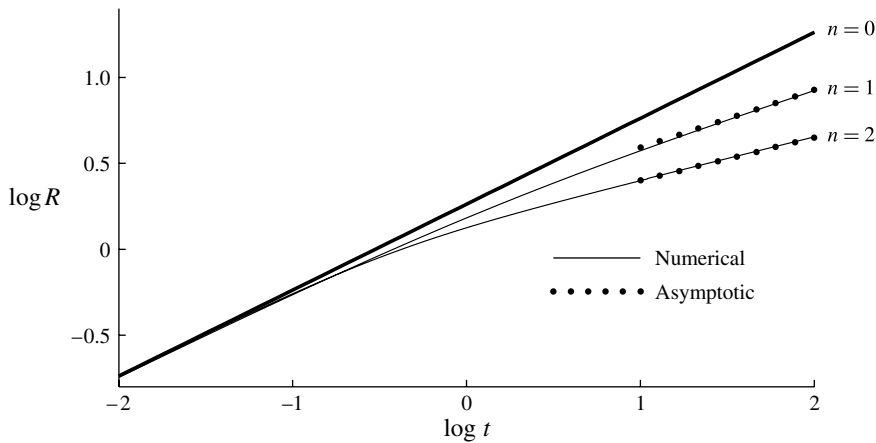
FIGURE 9. The evolution of the frontal position $R(t)$ for $n = 0$ (bold) and $n = 1$ and 2 (each thin) as a function of time for the axisymmetric flow produced by a point source at $r = 0$. The case $n = 0$ is described analytically by the similarity solution (4.11) at all times. The solutions for $n = 1$ and 2, which we have determined numerically, are seen to evolve from the similarity solution (4.11b) at early times towards the asymptote (4.13b) (dotted) at late times, illustrating the transition towards a regime in which the top surface of the current has become close to horizontal.
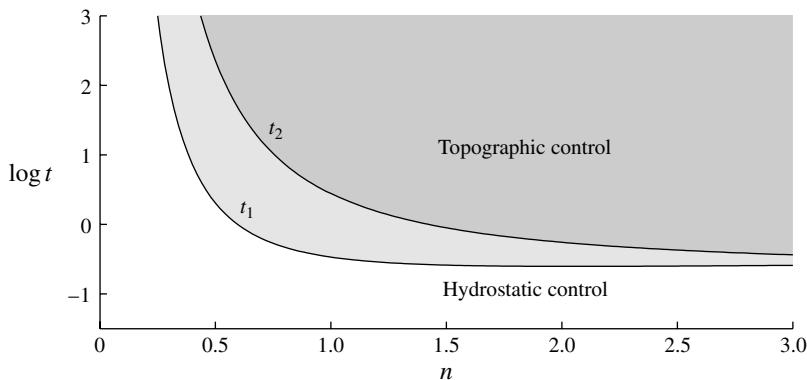

FIGURE 10. Characteristic dimensionless times t_1 and t_2, as defined by (3.12a,b), at which the flow transitions from the early-time similarity solution (4.11) to the late-time horizontally topped regime (4.13). Times at which the flow is controlled by hydrostatic spreading (white) and topographically controlled (heavily shaded) are separated by an intermediate region (lightly shaded) in which both hydrostatic spreading and topographic control are comparable.

This minimum is extremely wide, being barely distinguishable in figure 10, showing that t_1 is essentially constant for $n \gtrsim 1.5$. Both t_1 and t_2 increase as $n \to 0$, implying that both the transition away from the similarity solution (4.11) and to the horizontally topped regime (4.13) occur at ever later times, with the intermediate interval between them ($t_1 < t < t_2$) having an increasingly longer duration. This is different from the two-dimensional case, where the transitions become reversed below a critical value ($n < 1/2$) and proceed to occur in the opposite limit of small time as $n \to 0$.

A more quantitative understanding of the variations in the rate of convergence towards (4.13) between values of n can be developed using similar asymptotic methods to those presented in § 3.1 above. Specifically, we substitute perturbation expansions of the same form (3.13), except with r and R in place of x and X, into (4.5)–(4.9), to determine that

$$\alpha \equiv \frac{2n}{n+2}, \quad F = F_0 + N \int_\eta^1 \frac{1 - \eta^2}{\eta(1 - \eta^n)} \, d\eta, \quad \int_0^1 \eta F \, d\eta = 0, \quad (4.15a,b,c)$$

where $N \equiv [n/2(n+2)]^\alpha$ and the constant of integration F_0 in (4.15b) can be evaluated up to quadrature by applying (4.15c). Here, the exponent of relative decay (4.15a) is positive for all $n > 0$, which is consistent with the unconditional convergence of the system towards a horizontally topped state over all such n. The asymptotic predictions of (4.15b) in the cases $n = 1$ and 2 are shown as dotted curves in figure 8(a,b), where they are seen to agree well with our numerical solutions at late times. Like the two-dimensional case, the flow in the case $n = 2$ converges more rapidly towards its asymptote than with $n = 1$, again reflecting the fact that the exponent of relative decay (4.15a) is an increasing function of n.

By expanding the integrand in (4.15b) in powers of η, neglecting all but the leading-order term and evaluating the integral, we determine the singular behaviour near the source,

$$F \sim N \ln(1/\eta) \quad (\eta \to 0). \tag{4.16}$$

This is a different form from the leading-order behaviour near the source implied directly by integration of the source condition (3.6), namely, $h \sim [\ln(1/r)]^{1/2}$ (Lyle *et al.* 2005; Vella & Huppert 2006), indicating that (4.16) strictly only applies outside a small radius from the source, whose scale becomes relatively smaller with time. This is consistent with the fact that the perturbation from a horizontally topped state, given by the radial form of (3.13), cannot provide an asymptotic description of the surface of the current near the singularity at the source. The weaker agreement between the asymptotic prediction and the numerical solutions shown in figure 8 also reflects this.

4.2. *Paraboloidal topography*

To explore the consequences of non-axisymmetric topography, we focus on the case of a paraboloidal dome, obtained by setting $m = n = 2$ in (4.6b). Such topography describes a large class of three-dimensional geometries with slopes that vary at different rates between the x- and y-directions, depending on the value of A, which is the general leading-order term in a Taylor expansion about the maximum of any topographic trap (cf. Bickle *et al.* 2007). The limiting case $A = 0$ corresponds to a channel of uniform parabolic cross-section (cf. Golding & Huppert 2010). With $A = 1$, it forms an axisymmetric dome, which is a special case ($n = 2$) of the problem considered in § 4.1. In the intermediate cases $0 < A < 1$, the topography forms a non-axisymmetric dome, with the steepest increase in topography in the y-direction. Cases with $A > 1$ can be made equivalent to those with $0 < A < 1$ by switching the x- and y-axes, so we neglect those with no loss of generality.

On extending the argument given in § 4.1 to three dimensions, it is clear that the similarity solution (4.11) describes the early-time flow for all cases of $A \geqslant 0$. We determine the subsequent evolution numerically by recasting the system in terms of the scaled coordinate system (ζ, θ, t), where $\zeta \equiv r/R(\theta, t)$, which maps the numerical domain onto a rectangle, and using the two-dimensional generalization of the implicit scheme described in § 3 above. In the rescaled coordinate system, we discretize

the domain onto a fixed, two-dimensional grid, with centred differences used to approximate the spatial derivatives of R and θ and symmetry conditions applied along $\theta = 0$ and $\pi/2$. Our numerical solutions for the evolution of the front of the current $R(\theta, t)$ in the two cases $A = 0$ and $1/2$ are shown by the white curves in figures 11(*a*) and 11(*b*), respectively. The height distributions of the currents $h(r, \theta, t)$ at the final times are indicated by the depth of the shading, with lighter shading corresponding to a larger height.

With $A = 0$, the shape of the front is seen to evolve from the circular form implied by the early-time, self-similar form (4.11*b*) towards an approximately parabolic shape that becomes increasingly elongated with time. At the final time shown, the height distribution $h(r, \theta, t)$ is approximately uniform across the width of the channel, but still has significant variation along its length in the x-direction. Between the source and the downstream flow, there is a transition region that matches the radial flow imposed at the source to the predominantly unidirectional flow downstream. By imposing a condition of uniform unidirectional flow across the width of the channel and prescribing an areal source in the plane of $x = 0$, Golding & Huppert (2010) show that, with these assumptions, the unidirectional flow can be described at all times by a similarity solution of the form

$$h = t^{1/4} f(x/X), \quad X \equiv R(0, t) = \xi_N t^{5/8}, \quad |y| \leqslant h^{1/2}, \qquad (4.17a,b)$$

where $\xi_N \approx 1.95$. Our numerically determined frontal position $R(\theta, t)$ is seen to converge towards the frontal locus implied by (4.17), shown by a dotted curve in figure 11(*a*), reflecting the fact that the downstream flow eventually loses information of the imposed radial flow at the source.

As shown in figure 11(*b*), the solution with $A = 1/2$ transitions towards a state in which the current is horizontally topped in both the x- and y-directions, implying that, like the two-dimensional cases with $n > 1/2$ and the axisymmetric cases with $n > 0$ considered in §§ 3 and 4.1 above, the leading-order propagation eventually becomes determined purely by geometry and the total volume of injected fluid. Setting $h = h_0(t)$ in (4.9) and applying (4.8*a*), we determine the height and extent of this regime as

$$h = h_0(t) \equiv \left(\frac{2\sqrt{A}t}{\pi}\right)^{1/2}, \quad R = R_0(\theta, t) \equiv \left(\frac{h_0(t)}{A\cos^2\theta + \sin^2\theta}\right)^{1/2}, \quad (4.18a,b)$$

respectively.

To measure the influence of topographic variation over time, we consider the evolution of the horizontal aspect ratio, or *elongation*, defined by $E(t) \equiv X(t)/Y(t)$, where $Y \equiv R(\pi/2, t)$ is the maximum extent of the current in the y-direction, which we plot as a function of time in figure 12 for a selection of A. The value of E is seen to evolve from the unitary value implied by the axisymmetric early-time flow described by (4.11) towards the late-time asymptote $E \sim 1.38t^{1/2}$ (dotted), which can be derived from (4.17). The approximate constancy of the late-time first-order correction $(E - 1.38t^{1/2}) \sim 0.24$ is due to the adjustment of the radial flow near the source towards unidirectional flow over a dimensionless distance of order unity. The frontal locus (4.18*b*), shown by the dotted curve in figure 11(*b*), describes an ellipse of constant elongation $E = A^{-1/2}$. Our numerically obtained evolutions of E in figure 12 are seen to evolve towards this asymptotic value ($E \sim A^{-1/2}$) at a rate which is faster for smaller values of A.
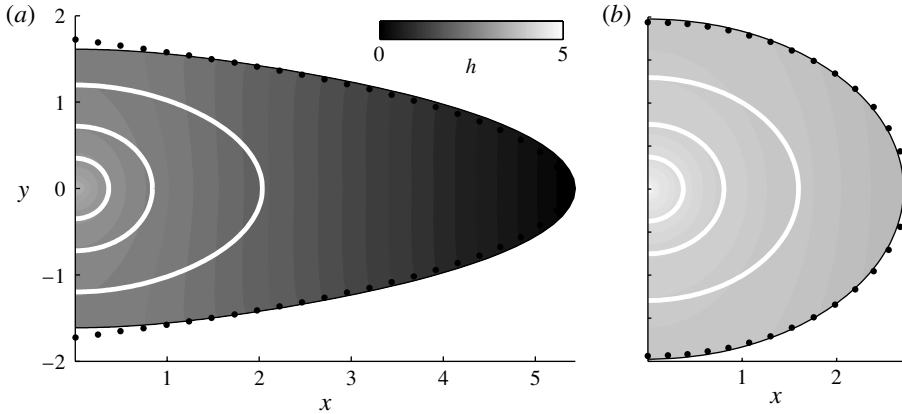
FIGURE 11. Height distribution $h(x, y, t)$ at time $t = 5$ for topographic curvature ratios of (*a*) $A = 0$, and (*b*) $A = 1/2$. In each case, the frontal locus $R(\theta, t)$ is shown at dimensionless times $t = 0.04, 0.2$ and 1 by the white curves. The frontal locus implied by the late-time asymptotic similarity solution (4.17) and the horizontally topped regime (4.18*b*) are shown as dotted curves in (*a*) and (*b*), respectively.
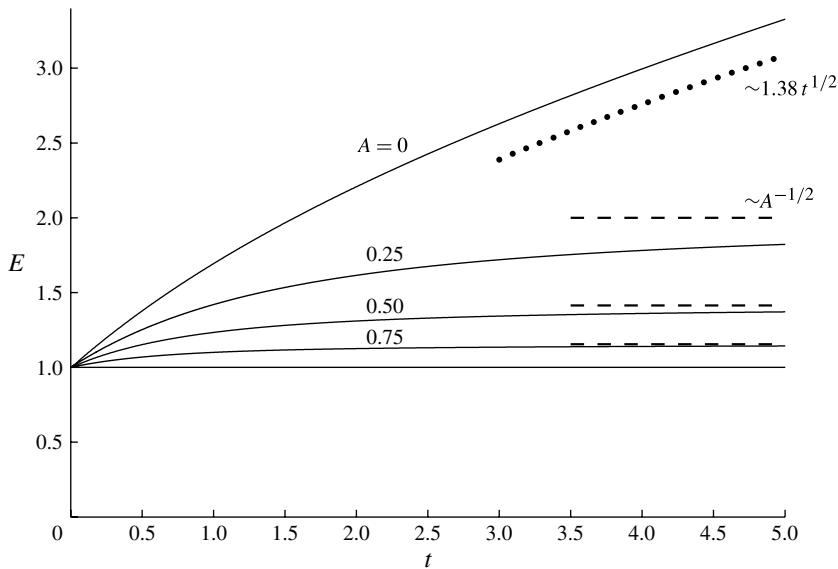

FIGURE 12. The elongation $E(t) \equiv X(t)/Y(t)$ as a function of time for a selection of topographic curvature ratios $A = 0, 0.25, 0.5, 0.75$ and 1. The late-time asymptote $1.38 \, t^{1/2}$ (dotted) for $A = 0$ and $A^{1/2}$ (dashed) for $A > 0$ are also plotted.

5. Geophysical application

Using the mathematical solutions we have developed, we can estimate the importance of topographic variations at the Sleipner field, where carbon dioxide is currently being sequestered. In that setting, the CO_2 is injected towards the base of the Utsira Sand, which is a sandstone layer with a thickness of 200 m and a top surface that lies about 800 m below ground level (Boait *et al.* 2012). The CO_2 is less dense

than the ambient brine, so it is initially driven vertically by buoyancy. The vertical propagation of the CO_2 towards the caprock is interrupted by a sequence of partially impermeable mudstone layers each with a typical thickness of a few metres, dividing the aquifer into a set of interstitial sandstone layers along which the CO_2 propagates with predominantly horizontal flow (Bickle *et al.* 2007; Arts *et al.* 2008; Boait *et al.* 2012). A significant proportion of the CO_2 leaks through the mudstone layers, such that there is a gradual migration of CO_2 towards the caprock, where no leakage occurs. Seismic measurements show that the CO_2 underneath each of these layers deviates significantly from axisymmetric flow (Bickle *et al.* 2007; Boait *et al.* 2012). By fitting ellipses to the data, Boait *et al.* (2012) find that the elongations E are approximately constant in several of the layers, with typical values of between 2 and 4, some of which have remained essentially constant since the initiation of the injection.

Data from seismic imaging show that the topography of the caprock forms a dome with its maximum centred relatively closely on the point of injection compared with the extents of the currents (Bickle *et al.* 2007; Arts *et al.* 2008; Boait *et al.* 2012). On this basis, we model the topography as a paraboloid ($m = n = 2$), as we considered theoretically in §4.2. To accommodate buoyancy into our theoretical model, we simply replace g by the reduced gravity $g' \equiv (\rho_w - \rho)g/\rho$, where $\rho_w > \rho$ is the density of the brine. By fitting parabolae along two perpendicular transects of the measured height of the top of the Utsira Sand (Arts *et al.* 2008), we estimate the smallest and largest topographic scales as $a \approx 5 \times 10^{-6}$ m^{-1} and $b \approx 10^{-5}$ m^{-1}, respectively. Given the porosity $\phi \approx 0.4$, permeability $k \approx 10^{-12}$ m^2, viscosity of carbon dioxide $\mu \approx 6 \times 10^{-5}$ Pa s, density of carbon dioxide $\rho \approx 700$ kg m^{-3}, density of brine $\rho_w \approx 1000$ kg m^{-3} and reduced gravity $g' \approx 4$ m s^{-2} typical at Sleipner (Boait *et al.* 2012), we estimate the time scale (4.3*c*) and the curvature ratio (4.10) as

$$\mathcal{T} \approx 20 \text{ years}, \quad A \approx 0.5, \qquad (5.1a,b)$$

respectively. With the value of A given by (5.1*b*), our solutions calculated in §4.2 predict that the difference between the elongation of the current and its starting value is within 90% of its asymptotic value $A^{-1/2} \approx 1.4$ at the dimensionless time $\hat{t} \approx 5$ (illustrated in figure 12). Combining this value with our estimate of the time scale (5.1*a*), we obtain the dimensional time at which this occurs as

$$t = \mathcal{T}\hat{t} \approx 100 \text{ years}. \qquad (5.2)$$

This time scale is one order of magnitude larger than the current sixteen-year running time of the Sleipner project, implying that the model predictions cannot explain the significant deviations of the currents from axisymmetric flow that have been observed there. Conversely, if the approximately constant elongations of $E \approx 4$ that have been observed in several of the layers were to be explained geometrically by the flow having approached a horizontally topped state with $E_0 \approx A^{-1/2}$, then the value of A needed ($A = E^{-2} \approx 0.06$) is two orders of magnitude smaller than that of the estimate (5.1*b*). With this value of A, the corresponding time scale $\mathcal{T}$ on which the elongation of the current approaches its asymptotic value would also be a few orders of magnitude larger than (5.2). The significance of these discrepancies indicates that a different physical property, such as the possible anisotropy of the permeability of the sandstone layer, may be the dominant cause of the observed departures from axisymmetric flow, and we intend to discuss this aspect in a subsequent publication.

6. Conclusions

We have determined the important time scales associated with the influence of upwards-sloping topography of power-law form on the dynamics of gravity currents in porous media. We considered both two- and three-dimensional geometries, showing in particular that the flows in these cases can exhibit qualitatively different transitional behaviour.

With two-dimensional flow produced at constant rate by a line source, we identified three distinct behaviours of the current, depending on whether the topographic exponent n satisfies $n > 1/2$, $n = 1/2$ or $n < 1/2$. If $n > 1/2$, then the current evolves from an early-time, self-similar form of extent $t^{2/3}$ towards a topographically controlled regime of extent $t^{1/(n+1)}$, which has a horizontally topped surface to leading order. This transition occurs once the current becomes predominantly constrained by the need to flow uphill. Asymptotic analysis of small perturbations to the horizontally topped regime reveals that they decay relative to it with temporal exponent $-(2n - 1)/(n + 1)$. In the critical case $n = 1/2$, the system is described by a similarity solution of extent $t^{2/3}$ in which the influences of hydrostatic spreading and topographic variation are comparable at all times. For $n < 1/2$, the transition between these two flow regimes is reversed, with a rapid early-time departure from a topographically controlled state towards a similarity solution that is insensitive to topographic variation. The theoretical predictions of the spreading rate in the case of a linear slope ($n = 1$) showed good agreement with the results of a series of laboratory experiments.

In the case of axisymmetric flow due to a point source, all non-zero values of the topographic exponents ($n > 0$) were shown to lead to a transition from a hydrostatically spreading similarity solution of extent $t^{1/2}$ towards a horizontally topped regime of extent $t^{1/(n+2)}$. Asymptotic analysis of perturbations to the late-time state showed that they decay relative to it with temporal exponent $-2n/(n + 2)$, implying a more rapid transition for larger values of n. In the case of a non-axisymmetric paraboloidal topography with ratio of the curvatures between its principle axes A, we identified two qualitatively distinct behaviours. If $A = 0$, corresponding to a channel of uniform cross-section, the current was shown to converge towards a similarity solution of unidirectional flow, which becomes increasingly elongated with time. If $A > 0$, it was shown to converge towards a horizontally topped regime of elliptic extent and constant elongation $A^{-1/2}$. The rate of convergence towards this late-time regime was shown to decrease with A, with the fastest rate of convergence occurring in the axisymmetric case $A = 1$.

The results of our analysis suggest that variations in the topography of the caprock are unlikely to have had any significant impact on the dynamics of CO_2 at the Sleipner field up to and somewhat beyond the present, and cannot explain the rapid deviations from axisymmetric flow that have been measured there.

REFERENCES

ARTS, R., CHADWICK, A., EIKEN, O., THIBEAU, S. & NOONER, S. 2008 Ten years' experience of monitoring CO_2 injection in the Utsira Sand at Sleipner, offshore Norway. *First Break* **26**, 65–72.

BARENBLATT, G. I. 1996 *Scaling, Self-Similarity, and Intermediate Asymptotics*. Cambridge University Press.

BEAR, J. 1988 *Dynamics of Fluids in Porous Media*. Dover.

BICKLE, M. J., CHADWICK, R. A., HUPPERT, H. E., HALLWORTH, M. A. & LYLE, S. 2007 Modelling carbon dioxide accumulation at Sleipner: implications for underground carbon storage. *Earth Planet. Sci. Lett.* **255**, 164–176.

BOAIT, F. C., WHITE, N. J., BICKLE, M. J., CHADWICK, R. A., NEUFELD, J. A. & HUPPERT, H. E. 2012 Spatial and temporal evolution of injected CO_2 at the sleipner field, north sea. *J. Geophys. Res.* **117**, B03309.

GOLDING, M. J. & HUPPERT, H. E. 2010 The effect of confining impermeable boundaries on gravity currents in a porous medium. *J. Fluid Mech.* **649**, 1–17.

GUNN, I. & WOODS, A. W. 2011 On the flow of buoyant fluid injected into a confined, inclined aquifer. *J. Fluid Mech.* **672**, 109–129.

HESSE, M. A., TCHELEPI, H. A., CANTWELL, B. J. & ORR, F. M. Jr 2007 Gravity currents in horizontal porous layers: transition from early to late self-similarity. *J. Fluid Mech.* **577**, 363–383.

HUPPERT, H. E. 1986 The intrusion of fluid mechanics into geology. *J. Fluid Mech.* **173**, 557–594.

HUPPERT, H. E. & WOODS, A. W. 1995 Gravity-driven flows in porous layers. *J. Fluid Mech.* **292**, 55–69.

DE LOUBENS, R. & RAMAKRISHNAN, T. S. 2011 Analysis and computation of gravity induced migration in porous media. *J. Fluid Mech.* **675**, 60–86.

LYLE, S., HUPPERT, H. E., HALLWORTH, M., BICKLE, M. & CHADWICK, A. 2005 Axisymmetric gravity currents in a porous medium. *J. Fluid Mech.* **543**, 293–302.

MITCHELL, V. & WOODS, A. W. 2006 Gravity driven flow in confined aquifers. *J. Fluid Mech.* **566**, 345–355.

NEUFELD, J. A., VELLA, D. & HUPPERT, H. E. 2009 The effect of a fissure on storage in a porous medium. *J. Fluid Mech.* **639**, 239–259.

NORDBOTTEN, J. M. & CELIA, M. A. 2006 Similarity solutions for fluid injection into confined aquifers. *J. Fluid Mech.* **561**, 307–327.

ORR, F. M. Jr 2009 Onshore geological storage of CO_2. *Science* **325**, 1656–1658.

PEGLER, S. S., KOWAL, K. N., HASENCLEVER, L. Q. & WORSTER, M. G. 2013 Lateral controls on grounding-line dynamics. *J. Fluid Mech.* **722**, R1.

VELLA, D. & HUPPERT, H. E. 2006 Gravity currents in a porous medium at an inclined plane. *J. Fluid Mech.* **555**, 353–362.